Photocatalytic activity of $PbTiO_3$ nanocrystals synthesized by hydrothermal method

SANYUAN LI[1], DESHENG SHI[1], ZHIXIONG HUANG[1], YAN QIN[1], DONGYUN GUO[1,*], YANG JU[2]
[1]*School of Materials Science and Engineering, Wuhan University of Technology, Wuhan 430070, China*
[2]*Department of Mechanical Science and Engineering, Nagoya University, Nagoya 464-8603, Japan*

$PbTiO_3$ nanocrystals were synthesized by a two-step hydrothermal method. The effect of Pb/Ti molar ratio (0.50 – 1.50) in the first-step precursors on morphologies of $PbTiO_3$ nanocrystals were investigated. The single-phase $PbTiO_3$ nanocrystals were obtained at Pb/Ti molar ratio of 0.75 – 1.25. By varying the Pb/Ti molar ratio from 0.75 to 1.50, the morphologies of $PbTiO_3$ nanocrystals changed from nanoparticles, to cubic nanocrystals, window-frame-like nanocrystals and nanoplates. The $PbTiO_3$ nanocrystals with cubic and window-frame-like morphologies showed good photocatalytic degradation of methylene blue under the visible-light irradiation.

(Received February 13, 2022; accepted June 6, 2022)

Keywords: $PbTiO_3$ nanocrystals, Hydrothermal method, Pb/Ti molar ratio, Morphology, Photocatalytic degradation

1. Introduction

As a typical pervoskite oxide, lead titanate ($PbTiO_3$) is one of the simplest ferroelectric oxides with high Curie temperature of 490 ^oC, which has potential applications in memory, capacitor, resonator and piezoelectric devices [1-3]. Recently, $PbTiO_3$ compound has attracted much attention due to its photocatalytic degradation of organic pollutions and photocatalytic splitting of water for the hydrogen production [4-10].

Arney et al. [4] synthesized $PbTiO_3$ particles in molten NaCl and PbO fluxes heated at 1000 ^oC for 1 h, and the roughly spherical and cubic $PbTiO_3$ particles were observed with sizes ranging from 100 to 6000 nm, and the Brunauer-Emmett-Teller (BET) surface areas ranging from 0.56 to 2.63 m^2/g. The water splitting photocatalytic activities of the $PbTiO_3$ particles were evaluated in visible light and yielded maximum rates of 27.4 $\mu mol \cdot H_2/(g \cdot h)$. Li et al. [5] synthesized $PbTiO_3$ particles by a hydrothermal method, and the $PbTiO_3$ particles could degrade about 91% of methyl orange after 180 min of illumination under simulated solar irradiation. Shabanalizadeh et al. [6] synthesized round $PbTiO_3$ nanoparticles with 45-55 nm in size by a sol-gel method, and the $PbTiO_3$ nanoparticles degraded about 97% of methyl orange after 60 min irradiation of ultraviolet light. Bhagwat et al. [7] synthesized $PbTiO_3$ nanorods by a sonochemical approach, and about 92% Congo red was degraded in 150 min at pH=6 in the existence of $PbTiO_3$ nanorods under visible light. Sun et al. [8] prepared Li-doped $PbTiO_3$ cubic particles by the hydrothermal method. They indicated that the Li-doping not only induced small size $PbTiO_3$ particles, but also brought about lots of Ti^{3+} ions and oxygen vacancies in the $PbTiO_3$ particles. Due to the formation of Ti^{3+} ions and oxygen vacancies, the Li-doped $PbTiO_3$ cubic particles showed excellent photocatalytic activities. Abirami et al. [9] prepared Ag-doped $PbTiO_3$ nanoparticles by hydrothermal method. The enhanced photocatalytic activity was obtained for Ag-doped $PbTiO_3$ nanoparticles, since Ag dopant effectively reduced the charge carrier recombination. Feng et al. [10] systematically studied the effects of charge separation and interfacial selectivity on photocatalytic performance of single-crystal $PbTiO_3$ nanoplates. They indicated that the strategy for charge separation and interfacial selectivity based on the synergistic effect of ferroelectricity and piezoelectricity could provide an idea for high-performance photocatalyst design and photocatalytic activity promotion in the field of photocatalytic CO_2 reduction, heavy ions reduction, volatile organic compounds removal and organic chemicals synthesis, beyond the area of photocatalytic contaminant degradation and H_2 generation. The grain size, morphologies, surface area and element-doping of $PbTiO_3$ compounds significantly influence their photocatalytic performance.

Hydrothermal method has been extensively applied in preparation of $PbTiO_3$ nanocrystals due to their low cost and low-temperature process with controllability of morphologies [11-15]. In this study, $PbTiO_3$ nanocrystals were synthesized by the hydrothermal method, and the ammonia solution was used as a pH-adjusting agent. By varying the Pb/Ti molar ratio in the precursors, the cubic and window-frame-like $PbTiO_3$ nanocrystals were synthesized and their photocatalytic properties were investigated.

2. Experimental details

2.1. Synthesis of $PbTiO_3$ nanocrystals

The reagents were of analytical grade purity and were used without further purification in this study. Lead acetate trihydrate ($(Pb(CH_3COO)_2 \cdot 3H_2O$), bis(ammonium lactate) titanium dihydroxide ($C_6H_{18}N_2O_8Ti$, TALH), ammonia solution and ethylene glycol were used as the starting materials. The desired amounts of $Pb(CH_3COO)_2 \cdot 3H_2O$ and $C_6H_{18}N_2O_8Ti$ were dissolved in deionized water with continuous stirring, and then the ammonia solution was added to form the suspended first-step precursors. In the first-step precursors, the Ti^{4+} concentration was kept at 0.05 mol/L, the nominal ammonia concentration was about 8.8 mol/L, and the Pb/Ti molar ratio was changed from 0.50 to 0.75, 1.00, 1.25 and 1.50. The precipitates were centrifuged and washed with deionized water. And then, these precipitates were dispersed in the deionized water, 10 ml ethylene glycol was added to the suspended solution as the surfactant, and the ammonia solution was added to form the 30 ml second-step precursors with nominal ammonia concentration of 4.4 mol/L. The second-step precursors were moved to Teflon-lined autoclaves of 50 ml capacity, they were sealed tightly and heated at 200 ^oC for 20 h, and then naturally cooled to room temperature with continuous stirring. The as-synthesized precipitates were centrifuged and washed with deionized water and ethanol in sequence.

2.2. Characterization

The phase composition of these precipitates was measured by an X-ray diffractometer (XRD, D/MAX-RB) with scanning speed of 2 ^{o}/min. The morphologies of $PbTiO_3$ nanocrystals were characterized by a field emission scanning electron microscope (FESEM, JSM-S4800) and a high-resolution transmission electron microscope (TEM, JEM-2100F). The absorption spectra of methylene blue solution were obtained using a UV-visible spectrophotometer (Shimadzu U-1240). The BET surface area of $PbTiO_3$ nanocrystals were analyzed using N_2 sorption experiments on a Micromeritics ASAP 2460 BET system.

2.3. Photocatalytic activity measurement

The photocatalytic activities of the cubic and window-frame-like $PbTiO_3$ nanocrystals were characterized by decomposing methylene blue under simulated solar irradiation at room temperature. An Xe illuminator (300 W) was used as an internal light source. The photodegradation experiments were carried out with the $PbTiO_3$ nanocrystals (50 mg) suspended in methylene blue aqueous solution (80 ml, 30 mg/L) with continuous stirring. The suspended solutions were stirred in the dark for 30 min to establish the adsorption/desorption equilibrium. At the given time intervals, 3 ml suspended solution was taken for analysis after centrifugation. The concentration of methylene blue was detected by measuring the absorption intensity at a wavelength of 664 nm. The absorption intensity was converted to the concentration of methylene blue referring to a standard curve which showed a linear relationship between the concentration and the adsorption intensity.

3. Results and discussion

Fig. 1 shows the XRD results of these precipitates synthesized at different Pb/Ti molar ratios in the first-step precursors. As the Pb/Ti molar ratio was 0.50, no obvious diffraction peak was observed. With increasing the Pb/Ti molar ratio to 0.75, a series of diffraction peaks were observed, which well coincided with pervoskite $PbTiO_3$ phase (JCPDS 78-0298, space group P4*mm*). When the Pb/Ti molar ratio ranged from 0.75 to 1.25, the single-phase $PbTiO_3$ precipitates could be obtained. At higher Pb/Ti molar ratio of 1.50, the impurity phase coexisted with $PbTiO_3$ phase.

Fig. 2 displays the typical morphologies of $PbTiO_3$ precipitates at different Pb/Ti molar ratios in the first-step precursors. When the Pb/Ti molar ratio was 0.75, the fine $PbTiO_3$ nanoparticles were formed. At Pb/Ti molar ratio of 1.00, the cubic $PbTiO_3$ nanocrystals were synthesized. The side length of cubic $PbTiO_3$ nanocrystals ranged from 100 to 140 nm, and the thickness was about 60 nm. With increasing the Pb/Ti molar ratio to 1.25, the window-frame-like $PbTiO_3$ nanocrystals were observed, and their thickness was about 30 nm. At higher Pb/Ti molar ratio of 1.50, $PbTiO_3$ precipitate mainly consisted of nanoplates, and the nanoplate thickness was also about 30 nm. In the first-step precursors, as the ammonia solution was added to the precursors, the $Ti(OH)_4$ colloids were formed with spatial network structure, and $Pb(OH)_2$ was dispersed in the $Ti(OH)_4$ colloids. At Pb/Ti molar ratio of 0.75 and 1.00, the $PbTiO_3$ nanocrystals grew up based on the $Ti(OH)_4$ spatial network structure, and the nanoparticles and cubic nanocrystals were formed. At high Pb/Ti molar ratio (1.25 and 1.50), the excess $Pb(OH)_2$ might destroy the $Ti(OH)_4$ spatial network structure to form the 2-dimensional structure, and the $PbTiO_3$ nanocrystals tended to grow up along the 2-dimensional direction to form the window-frame-like and nanoplate morphologies.

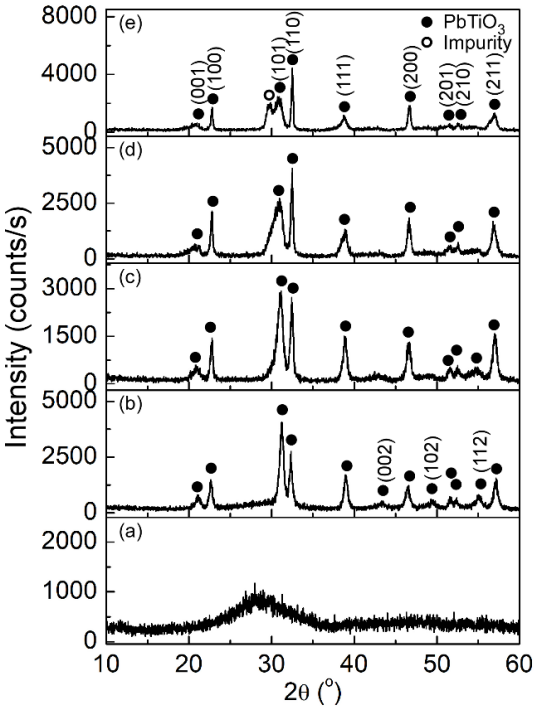

Fig. 1. XRD patterns of the precipitates synthesized at different Pb/Ti molar ratios: (a) 0.50, (b) 0.75, (c) 1.00, (d) 1.25 and (e) 1.50

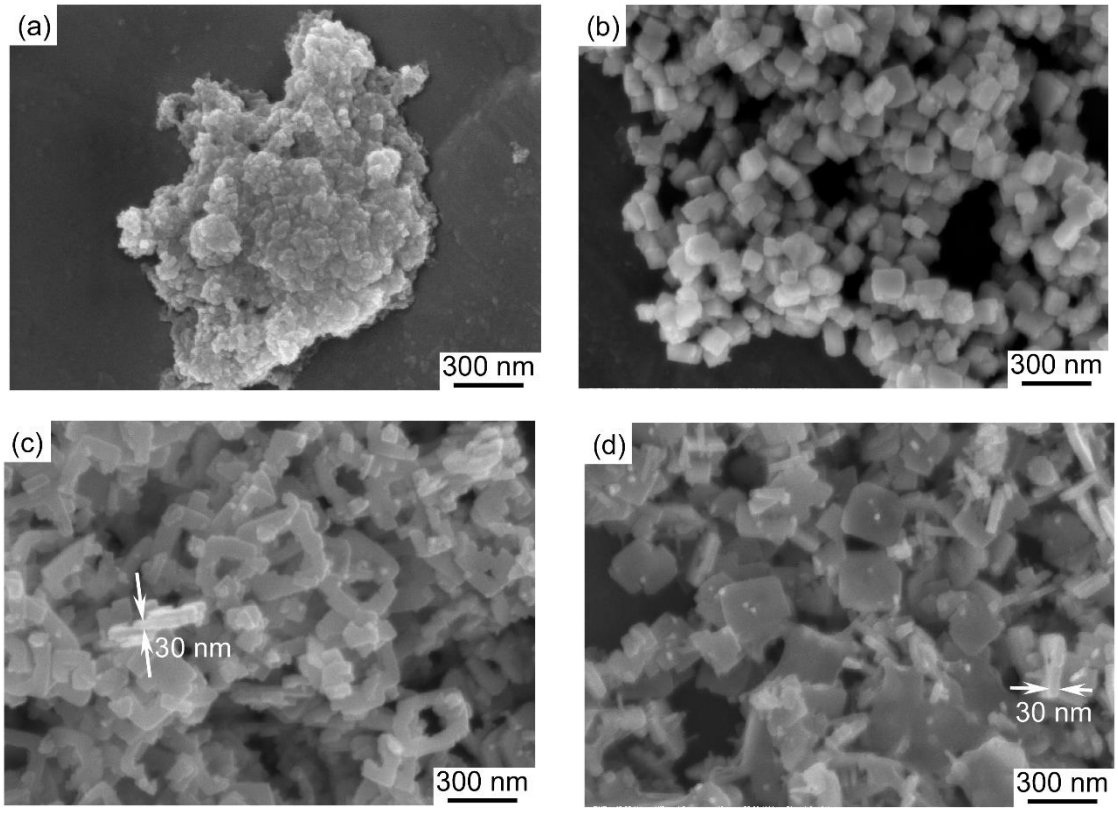

Fig. 2. Morphologies of $PbTiO_3$ nanocrystals synthesized at different Pb/Ti molar ratios: (a) 0.75, (b) 1.00, (c) 1.25 and (d) 1.50

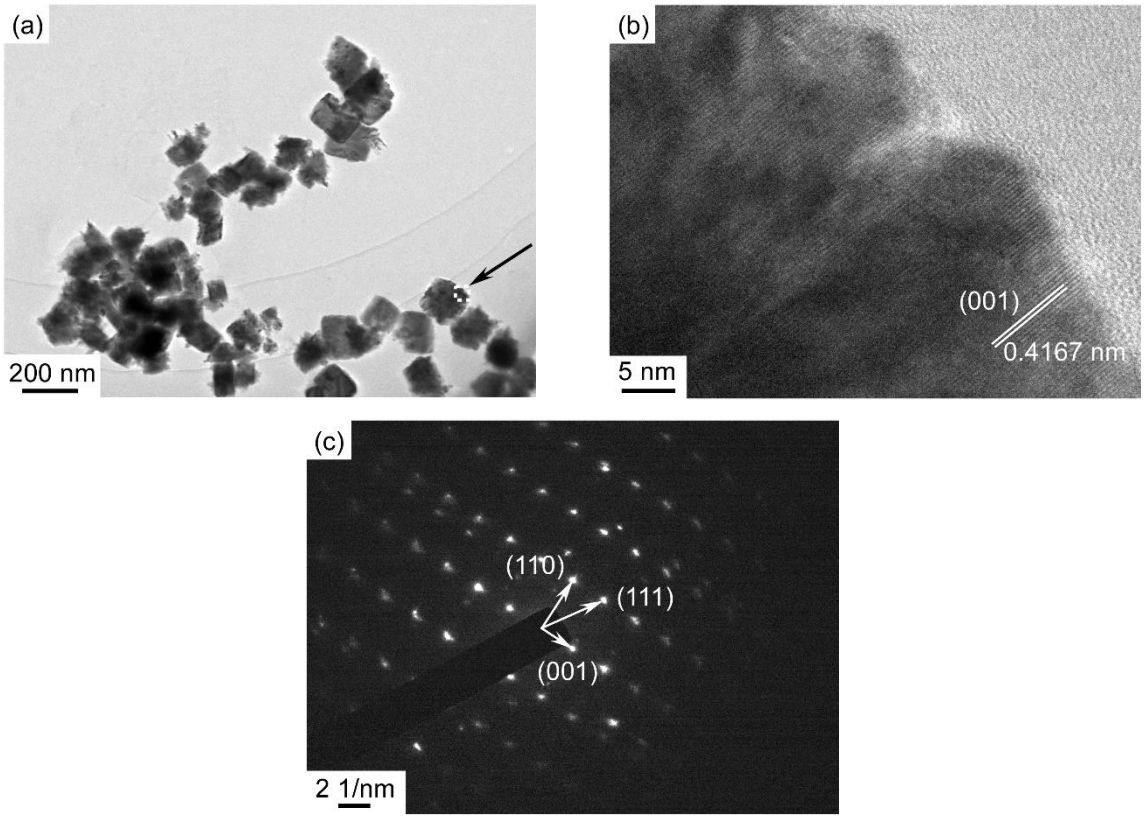

Fig. 3. TEM image (a) of cubic $PbTiO_3$ nanocrystals synthesized at Pb/Ti molar ratio of 1.00, high-resolution TEM image (b) corresponding to the circled area in (a), and its corresponding selected area electron diffraction (SAED) pattern (c)

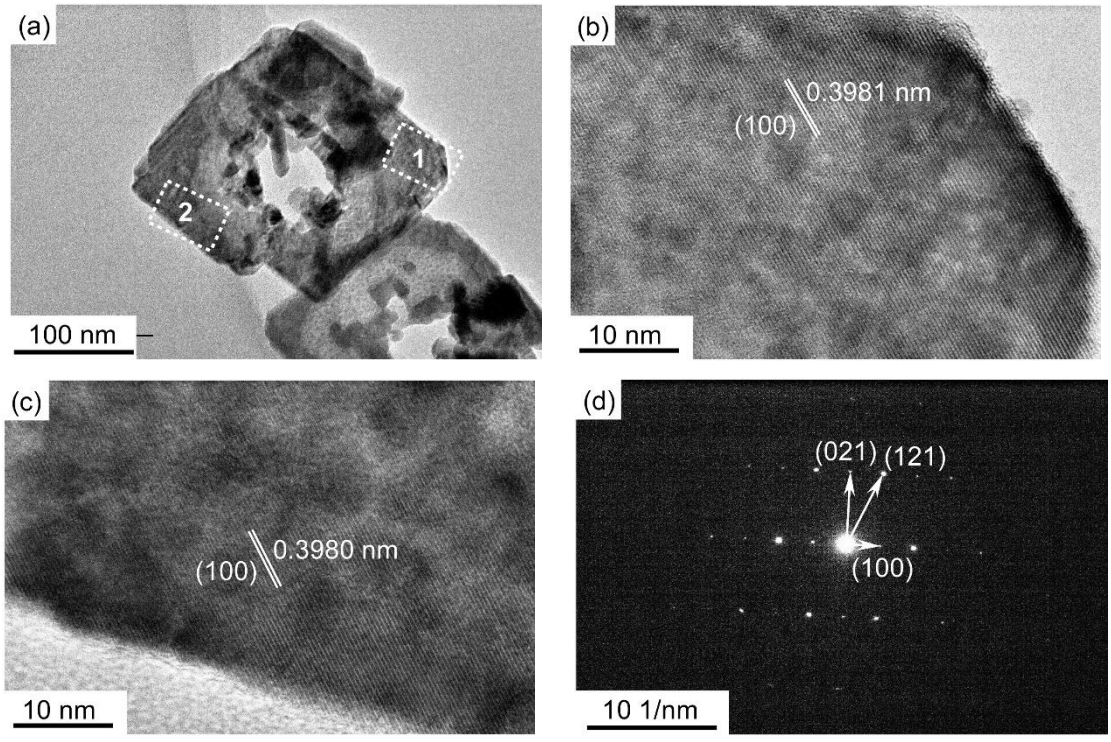

Fig. 4. TEM image (a) of window-frame-like $PbTiO_3$ nanocrystals synthesized at Pb/Ti molar ratio of 1.25, high-resolution TEM images (b and c) corresponding to areas 1 and 2 in (a), and its corresponding SAED pattern (d)

To further identify the phase composition of cubic and window-frame-like nanocrystals, they were analyzed by the TEM technique. Fig. 3 shows the TEM result of cubic $PbTiO_3$ nanocrystals. The cubic $PbTiO_3$ nanocrystals were clearly observed in Fig. 3(a). Fig. 3(b) shows the high-resolution TEM image of the circled area in Fig. 3(a). The clear lattice fringes were observed due to high crystallinity of the cubic $PbTiO_3$ nanocrystal, and the interplanar distances of 0.417 nm corresponded to (001) plane of tetragonal $PbTiO_3$ phase. Its corresponding SAED pattern is shown in Fig. 3(c). The measuring angles between (110) and (001) planes, (110) and (111) planes were 90.16^o and 33.01^o, respectively. The calculated angles between (110) and (001) planes, (110) and (111) planes of tetragonal $PbTiO_3$ phase (JCPDS 78-0298) were 90^o and 33.57^o, respectively. The values of calculated angles were very close to those of measuring angles, which indicated that the cubic nanocrystals belonged to the single-crystal tetragonal $PbTiO_3$ phase. The TEM result of window-frame-like nanocrystals is shown in Fig. 4. Fig. 4(a) shows a whole window-frame-like nanocrystal. The high-resolution TEM images of area 1 and 2 in Fig. 4(a) are shown in Figs. 4(b) and (c). The clear lattice fringes were observed with interplanar distances of 0.398 nm corresponding to (100) or (010) planes of tetragonal $PbTiO_3$ phase. According to the SAED pattern in Fig. 4(d), the measuring angles between (021) and (100) planes, (021) and (121) planes were 90.15^o and 24.58^o, respectively. The calculated angles between (021) and (100) planes, (021) and (121) planes of tetragonal $PbTiO_3$ phase (JCPDS 78-0298) were 90^o and 24.35^o, respectively. The values of calculated angles were very close to those of measuring angles. The SAED pattern further confirmed that the window-frame-like nanocrystals also belonged to the tetragonal $PbTiO_3$ phase.

Photocatalytic activity of the cubic and window-frame-like $PbTiO_3$ nanocrystals was evaluated by the degradation of methylene blue in the aqueous solutions under the visible-light irradiation. The concentration of methylene blue was monitored by examining the variations of typical absorption spectra of methylene blue at 664 nm. Fig. 5 displays the absorption spectra of the methylene blue solution with the visible-light irradiation under the effect of $PbTiO_3$ nanocrystals, and photocatalytic degradation with different irradiation time. The methylene blue was continuously removed by the cubic and window-frame-like $PbTiO_3$ nanocrystals under visible-light irradiation. Both $PbTiO_3$ nanocrystals showed good photocatalytic performance on the degradation of methylene blue under the visible-light irradiation. After the visible-light irradiation for 3 h, the photocatalytic degradation of methylene blue with the cubic $PbTiO_3$ nanocrystals was about 66.0%, and the photocatalytic degradation of methylene blue with the window-frame-like $PbTiO_3$ nanocrystals achieved 66.5%. It is well known that the photocatalytic performance of $PbTiO_3$ compounds was influenced by grain size, morphologies, surface area and element-doping [4-10].

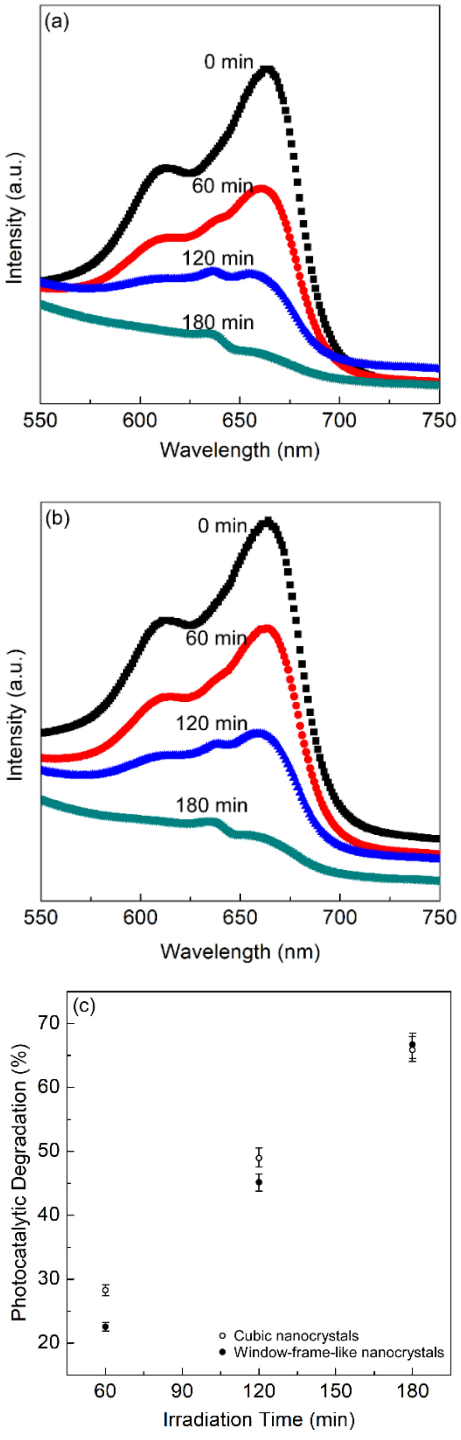

Fig. 5. Absorption spectra of cubic (a) and window-frame-like (b) $PbTiO_3$ nanocrystals in the methylene blue aqueous solutions depended on time under the visible-light irradiation, and (c) photocatalytic degradation of methylene blue in the aqueous solutions by $PbTiO_3$ nanocrystals with different irradiation time (color online)

However, in this study, even the grain size and morphologies of the cubic and window-frame-like $PbTiO_3$ nanocrystals varied widely, their photocatalytic degradation was almost the same. The small difference of photocatalytic degradation might be attributed to the similar surface area of $PbTiO_3$ nanocrystals. The BET surface area of the cubic $PbTiO_3$ nanocrystals was about 20.7928 m^2/g, and that of the window-frame-like $PbTiO_3$ nanocrystals was about 21.0809 m^2/g. This results indicated that the surface area played the most important role in the photocatalytic activity of $PbTiO_3$ nanocrystals.

4. Conclusions

The $PbTiO_3$ nanocrystals with different morphologies were synthesized by varying the Pb/Ti molar ratio in the first-step precursors. The single-phase $PbTiO_3$ nanocrystals were obtained as the Pb/Ti molar ratio ranged from 0.75 to 1.25. With increasing the Pb/Ti molar ratio from 0.75, to 1.50, the nanoparticles, cubic nanocrystals, window-frame-like nanocrystals and nanoplates could be formed. The $PbTiO_3$ nanocrystals with cubic and window-frame-like morphologies showed good photocatalytic performance.

Acknowledgement

This work was supported by the National Natural Science Foundation of China (Grant No. 51272195).

References

[1] T. Yanagitani, S. Takayanagi, Jpn. J. Appl. Phys. **60**, SD0803 (2021).
[2] S. Zhang, F. Li, X. Jiang, J. Kim, J. Luo, X. Geng, Prog. Mater. Sci. **68**, 1 (2015).
[3] Y. Tang, Y. Zhu, X. Ma, A. Y. Borisevich, A. N. Morozovska, E. A. Eliseev, W. Wang, Y. Wang, Y. Xu, S. Zhang, S. Pennycook, Science **348**, 547 (2015).
[4] D. Arney, T. Watkins, P. A. Maggard, J. Am. Ceram. Soc. **94**, 1483 (2011).
[5] Y. Li, H. Sun, N. Wang, W. Fang, Z. Li, Solid State Sci. **37**, 18 (2014).
[6] S. Shabanalizadeh, A. Abedeini, A. Alborzi, M. Bahmani, N. Shaghaghi, S. Hajebi, M. Yazdanmehr, J. Mater. Sci.: Mater. Electron. **27**, 2589 (2016).
[7] U. O. Bhagwat, J. J. Wu, A. M. Asiri, S. Anandan, Chemistry Select. **3**, 11851 (2018).
[8] X. Sun, S. Deng, Y. Yang, G. Xu, R. Zhao, G. Shen, G. Han, Surf. Coat. Tech. **320**, 527 (2017).
[9] R. Abirami, T. S. Senthil, S. Kalpana, L. Kungumadevi, M. Kang, Mater. Lett. **279**, 128507 (2020).
[10] Y. Feng, M. Xu, H. Liu, W. Li, H. Li, Z. Bian, Nano Energy **73**, 104768 (2020).
[11] X. Li, Z. Huang, L. Zhang, D. Guo, Electron. Mater. Lett. **14**, 610 (2018).
[12] X. Li, J. Yue, Z. Huang, L. Zhang, D. Guo, Y. Ju, J. Mater. Sci.: Mater. Electron. **31**, 12345 (2020).
[13] J. Yue, Z. Huang, D. Guo, Y. Ju, Optoelectron. Adv. Mat. **15**, 504 (2021).
[14] H. Tang, Z. Zhou, C. C. Bowland, H. A. Sodano, Nanotechnology **26**, 345602 (2015).
[15] E. H. Lahrar, O. El Ghadraoui, M. Zouhairi, A. Harrach, T. Lamcharfi, E. H. El Ghadraoui, New J. Chem. **45**, 13293 (2021).

*Corresponding author: guody@whut.edu.cn